Supporting Information:

Unusual Li-ion Intercalation Activation With Progressive Capacity Increase in Orthosilicate Nanocomposite Cathode

Majid Rasool[a], Hsien-Chieh Chiu[a], Raynald Gauvin[a], De-Tong Jiang[b, c], Jigang Zhou[c], Dominic Ryan[d], Karim Zaghib[e], and George P. Demopoulos*[a]

a. Materials Engineering, McGill University, Montreal, QC H3A 0C5, Canada
b. Department of Physics, University of Guelph, Guelph, ON N1G 2W1, Canada
c. Canadian Light Source, Saskatoon, SK S7N 2V3, Canada
d. Department of Physics, McGill University, 3600 Rue University, Montreal, QC H3A 2T8, Canada
e. Centre d'excellence-ETSE, Hydro-Québec, Varennes, QC, Canada

*Corresponding author: Phone: 514-398-2046; Fax: 514-398-4492; **ORCID** #0000-0001-8112-5339; Email: george.demopoulos@mcgill.ca

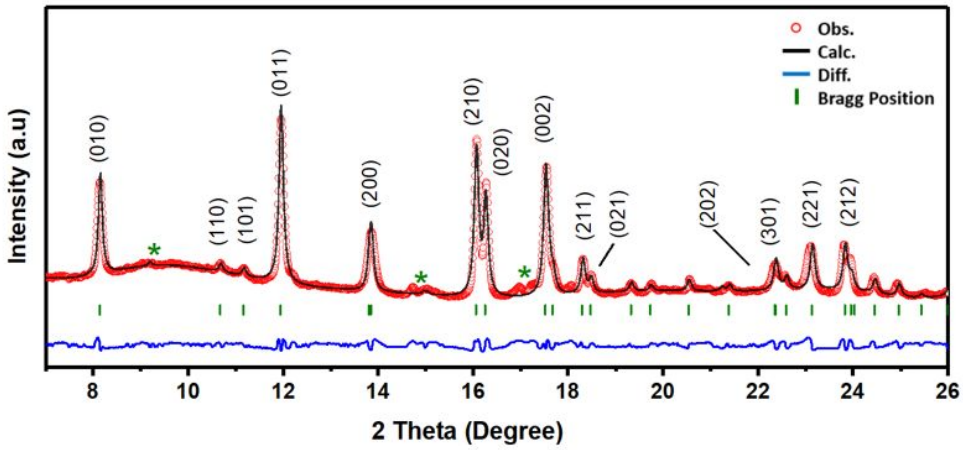

Figure S1: XRD pattern of as-prepared Li_2FeSiO_4 sample obtained with synchrotron source (λ = 0.7523 Å) and refined with *Pmn2₁* space group (R_{wp} = 4.60, R_p = 3.51 and GOF = 2.95) using TOPAS software. Lattice parameters obtained from fitting are a = 6.2691995 (Å), b = 5.3429072 (Å) and c = 4.956382 (Å). The '*' indicate the presence of minor iron oxide impurities (Fe_2O_3, Fe_3O_4 and $Fe(OH)_3$). By comparing the relative peak areas, the iron oxides were estimated to amount to about ~5% of the LFs material.

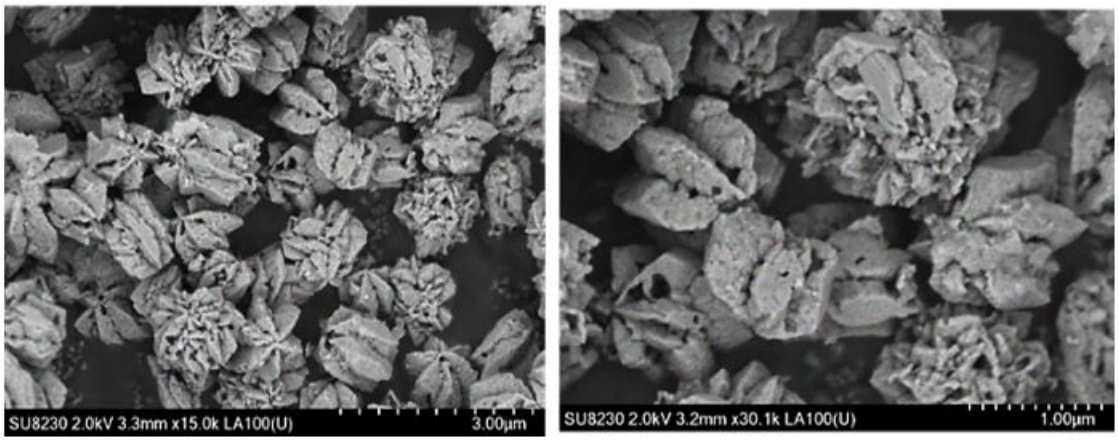

Figure S2: SEM images of as-prepared Li_2FeSiO_4 by hydrothermal synthesis at 200°C at different resolutions.

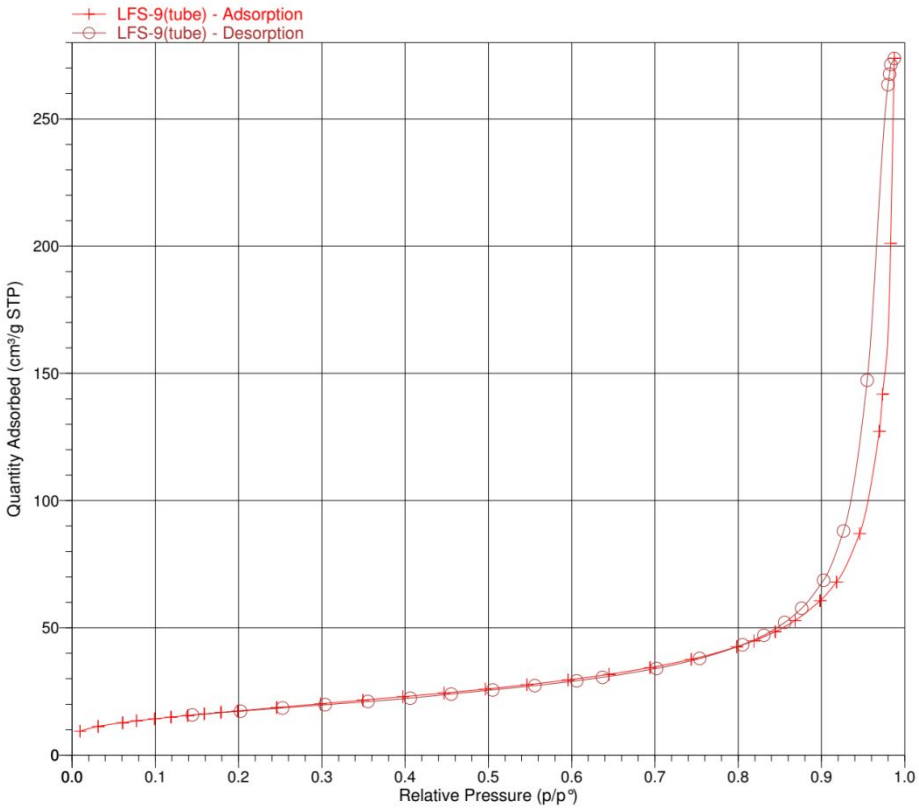

Figure S3: Nitrogen adsorption-desorption isotherm plot of LFS@C nanocomposite sample after mechanochemical treatment in the presence of carbon.

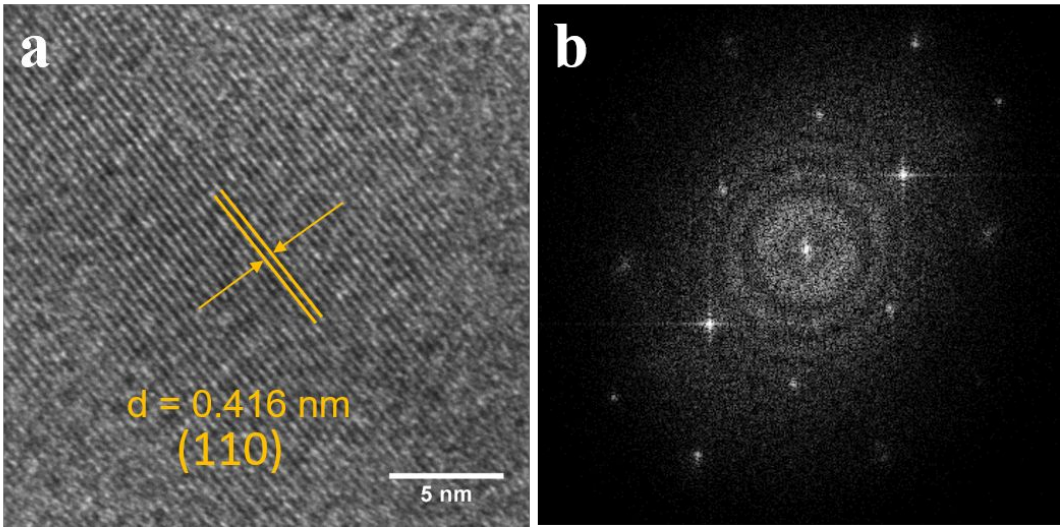

Figure S4: (a) HRTEM of LFS@C nanocomposite and its corresponding (b) fast Fourier transform (FFT) obtained using Image J software, respectively.

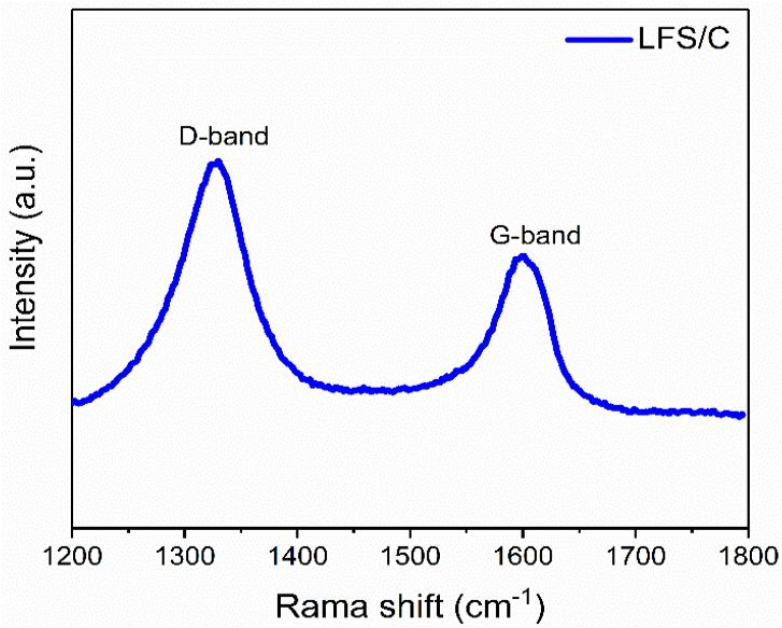

Figure S5: Raman spectroscopy indicating D and G bands for carbon presence in LFS@C nanocomposite sample.

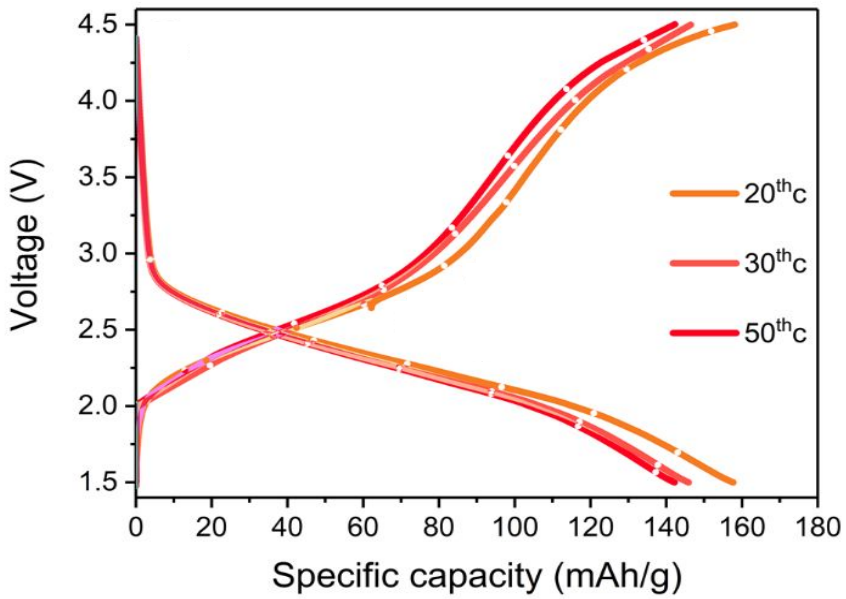

Figure S6: (e) Charge/discharge plots after 20, 30 and 50th cycle of LFS@C nanocomposite at C/50.

Table S1: EIS fitting results for LFS@C nanocomposite.

Sample	R_S (Ω)	R_{SEI}(Ω)	R_{CT} (Ω)
LFS – c2	8.1	15.2	118.3
LFS – c11	8.3	29.5	92.3
LFS – c20	8.2	35.2	79.4
LFS – c50	8.3	39.3	48.3

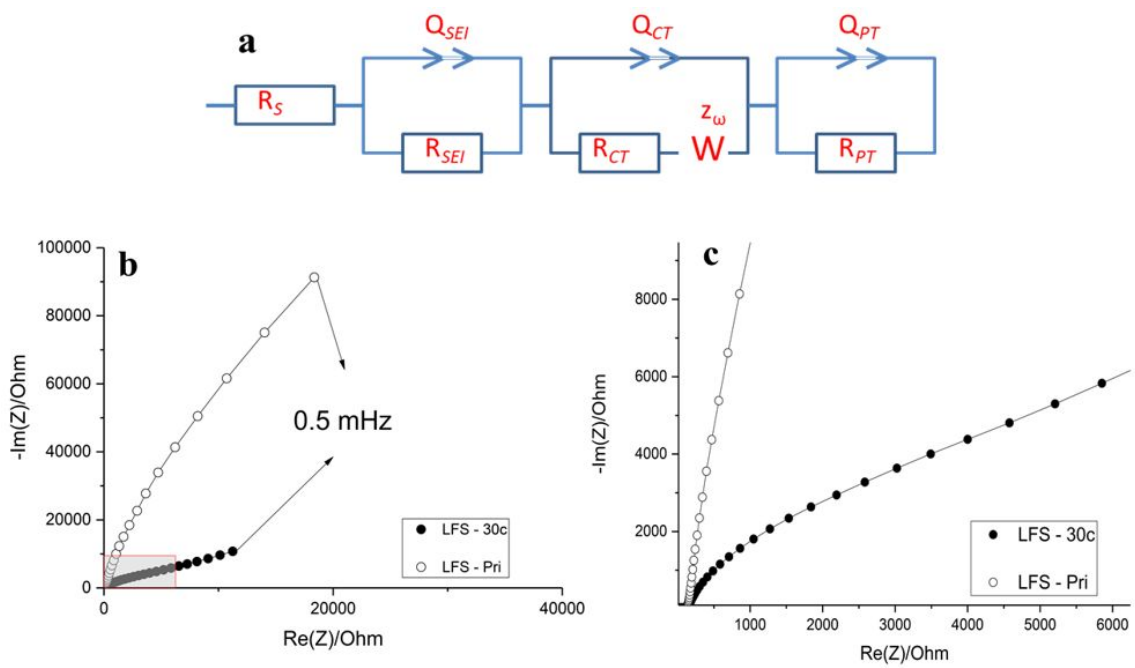

Figure S7: EIS comparison at a very low frequency (0.5 mHz) between pristine LFS@C nanocomposite electrode and after 30th cycle. (a) Equivalent circuit model used to obtain the results, notably, where R_{PT} (Ω) denotes the phase transition during cycling [1-3]. (b) White open circle symbol corresponds to EIS of freshly assembled LFS@C electrode. Black solid circles correspond to cycled LFS@C electrode after 20th cycle. It can be clearly seen that the intercalation kinetics are changed completely after cycling. Obtained results are present in Table S2 below. R_{PT} (Ω) has reduced significantly after in-situ electrochemical phase transition. (c) An enlarged plot of red box shown in (b).

Table S1: EIS fitting results for pristine LFS@C nanocomposite electrode and after 30th discharge cycle.

Sample	R_S (Ω)	R_{SEI}(Ω)	R_{CT} (Ω)	R_{PT} (Ω)
LFS – Pristine	8.3	4.3	127.9	87,010
LFS – c30	8.2	41.2	86.2	10,254

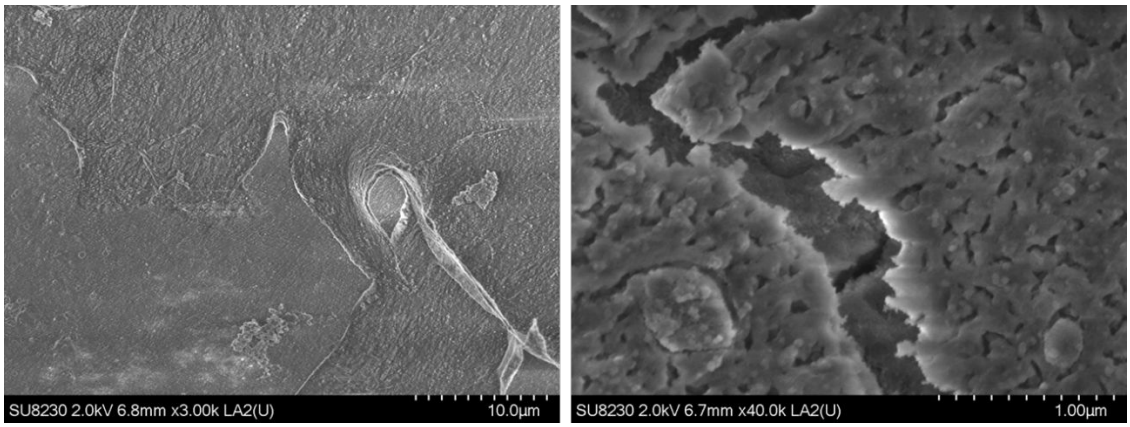

Figure S8: SEM image of *ex-situ* electrode of LFS@C nanocomposite at different resolutions after 30th cycle, where cracks were introduced during handling.

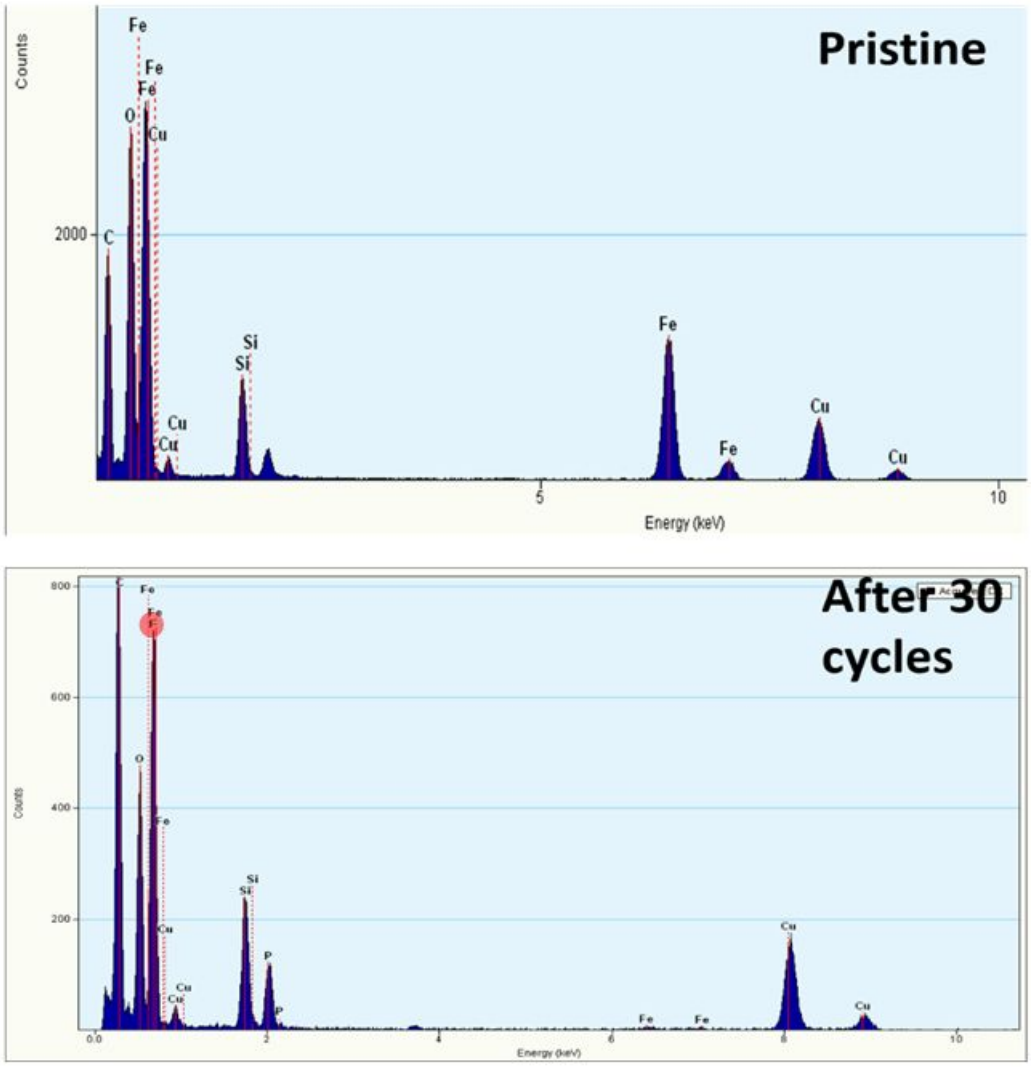

Figure S9: Energy-dispersive X-ray spectroscopy (EDS) maps of pristine LFS@C nanocomposite electrode vs. after 30 cycles of galvanostatic charging/discharging collected along with TEM.

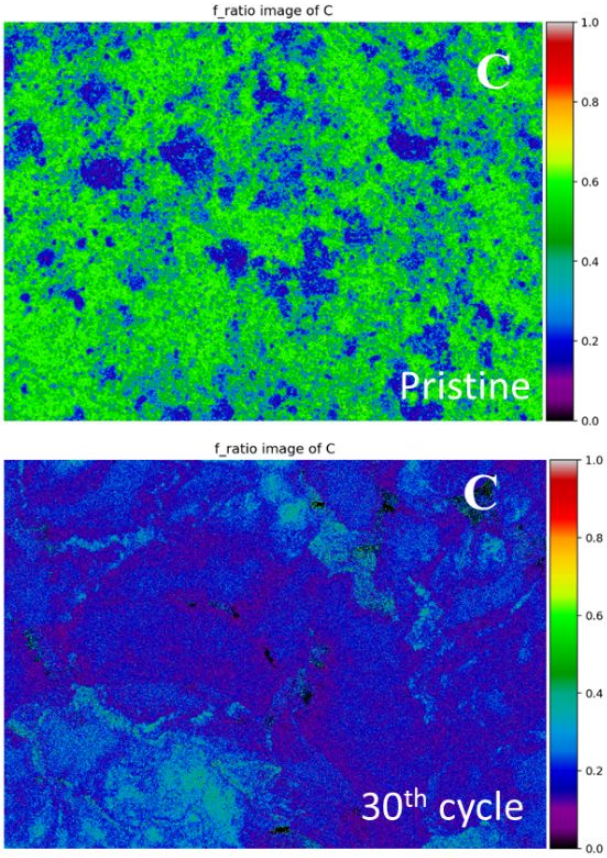

Figure S10 : *f*-ratio maps for Carbon are shown for pristine LFS@C nanocomposite electrode and after 30th discharge cycle.

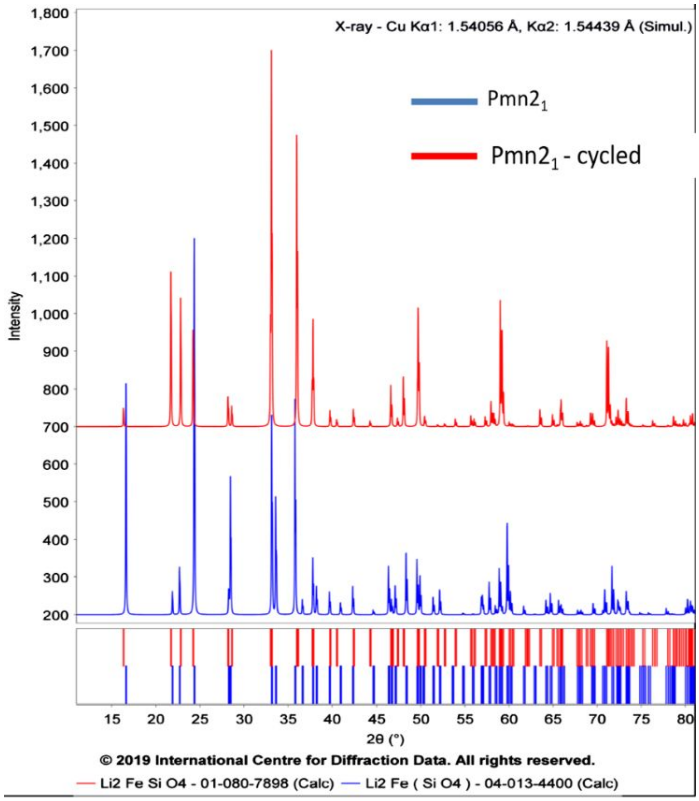

Figure S11: Simulation of normal *Pmn2$_1$* phase and inverse *Pmn2$_1$* (or "cycled") of Li_2FeSiO_4 obtained via PDF-4+ 2019 software.

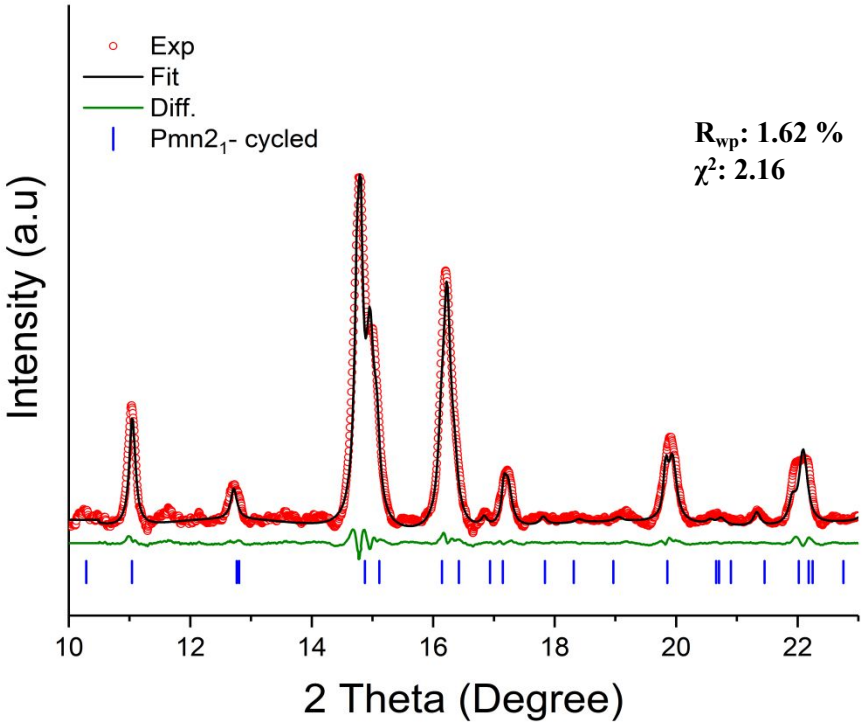

Figure S12: Le-Bail fitting results obtained for LFS@C nanocomposite after 30 cycles (collected at discharge state) via TOPAS software. Lattice parameters obtained from fitting are a = 6.2421(3) (Å), b = 5.3924(7) (Å) and c = 5.0119(5) (Å).

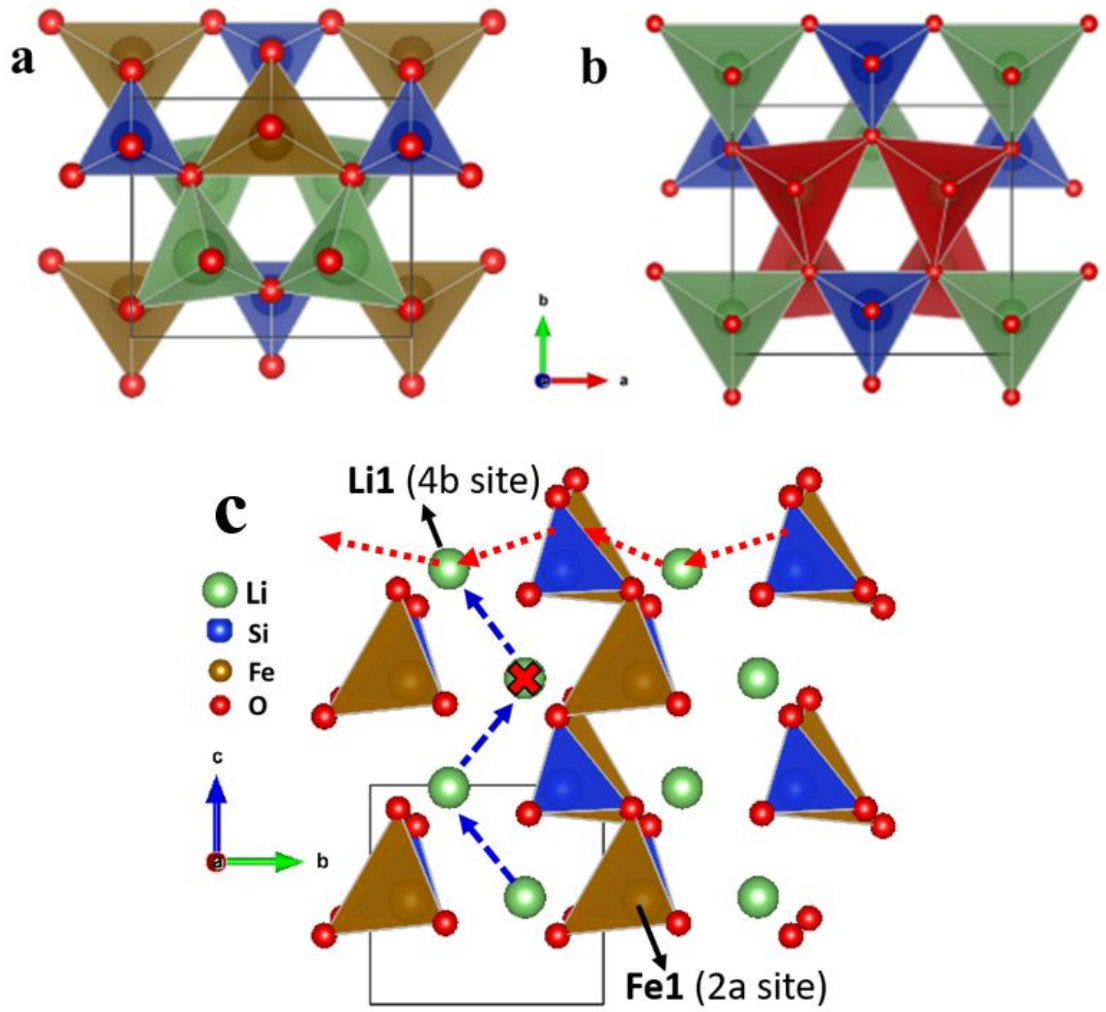

Figure S13: Illustrations of crystal structure models drawn by Vesta Software. (a) *Pmn2₁* phase of LFS, where all tetrahedra point towards the same direction. Li-ions can migrate along only in two directions. (b) In the inverse $Pmn2_1$ (electrochemically cycled structure), where all the Fe-ions exchange site with half of the Li2-site, Li-ions can migrate along in three different directions [4]. (c) For a visual aid, crystal structure was drawn without tetrahedra of Lithium, where Li and Fe atoms occupy different crystallographic sites in the ideal $Pmn2_1$ structure of Li_2FeSiO_4, denoted as Li1 (4b site) and Fe1 (2a site), respectively [4-5]. During electrochemical lithiation/de-lithiation, Li migrates in either a-direction (into the paper as denoted by the red cross) or a zig-zag c-direction (denoted by blue arrows). After cycling, significant cation mixing occurred, a new pathway opens up and the lithium can diffuse into zig-zag b-direction (red-arrows) as well.

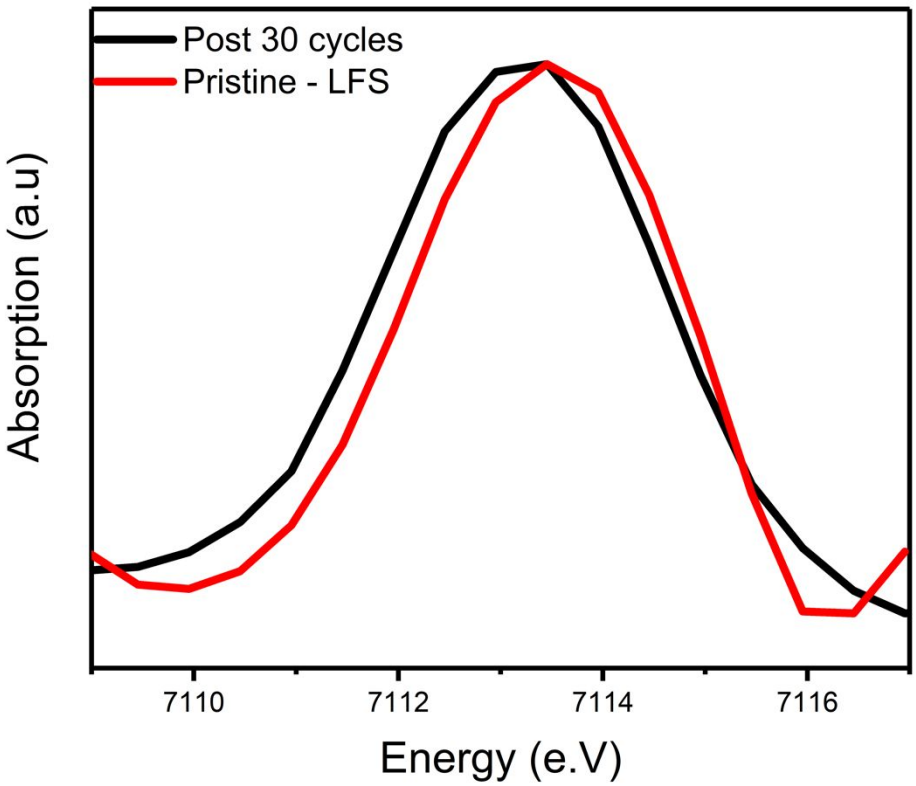

Figure S14: Zoomed-in pre-edge of XANES Iron K-edge spectra of pristine LFS@C nanocomposite electrode and after 30 cycles, the background was subtracted using Origin software.

References:

1. Orazem, M. E.; Tribollet, B., *Electrochemical impedance spectroscopy*. John Wiley & Sons: 2017.

2. Sen, U. K.; Johari, P.; Basu, S.; Nayak, C.; Mitra, S., An experimental and computational study to understand the lithium storage mechanism in molybdenum disulfide. *Nanoscale* **2014,** *6* (17), 10243-10254.

3. Shaju, K.; Rao, G. S.; Chowdari, B., Li ion kinetic studies on spinel cathodes, $Li(M_{1/6}Mn_{11/6})O_4$ (M= Mn, Co, CoAl) by GITT and EIS. *Journal of Materials Chemistry* **2003,** *13* (1), 106-113.

4. Armstrong, A. R.; Kuganathan, N.; Islam, M. S.; Bruce, P. G., Structure and Lithium Transport Pathways in Li_2FeSiO_4 Cathodes for Lithium Batteries. *J. Am. Chem. Soc.* **2011,** *133* (33), 13031-13035.

5. Liivat, A.; Thomas, J. O., Li-ion migration in Li_2FeSiO_4-related cathode materials: A DFT study. *Solid State Ion.* **2011,** *192* (1), 58-64.